ARTICLE

doi:10.1038/nature16526

# High-fidelity CRISPR–Cas9 nucleases with no detectable genome-wide off-target effects

Benjamin P. Kleinstiver[1,2]*, Vikram Pattanayak[1,2]*, Michelle S. Prew[1], Shengdar Q. Tsai[1,2], Nhu T. Nguyen[1], Zongli Zheng[3] & J. Keith Joung[1,2]

**CRISPR–Cas9 nucleases are widely used for genome editing but can induce unwanted off-target mutations. Existing strategies for reducing genome-wide off-target effects of the widely used *Streptococcus pyogenes* Cas9 (SpCas9) are imperfect, possessing only partial or unproven efficacies and other limitations that constrain their use. Here we describe SpCas9-HF1, a high-fidelity variant harbouring alterations designed to reduce non-specific DNA contacts. SpCas9-HF1 retains on-target activities comparable to wild-type SpCas9 with >85% of single-guide RNAs (sgRNAs) tested in human cells. Notably, with sgRNAs targeted to standard non-repetitive sequences, SpCas9-HF1 rendered all or nearly all off-target events undetectable by genome-wide break capture and targeted sequencing methods. Even for atypical, repetitive target sites, the vast majority of off-target mutations induced by wild-type SpCas9 were not detected with SpCas9-HF1. With its exceptional precision, SpCas9-HF1 provides an alternative to wild-type SpCas9 for research and therapeutic applications. More broadly, our results suggest a general strategy for optimizing genome-wide specificities of other CRISPR-RNA-guided nucleases.**

CRISPR–Cas9 nucleases enable highly efficient genome editing in a wide variety of organisms[1–3], but can also cause unwanted mutations at off-target sites that resemble the on-target sequence[4–13]. These off-target effects can confound research experiments and also have potential implications for therapeutic uses of the technology. Various strategies have been described to reduce genome-wide off-target mutations of the commonly used SpCas9 nuclease, including: truncated sgRNAs bearing shortened regions of target site complementarity[8,14], SpCas9 mutants such as the recently described D1135E variant[15], paired SpCas9 nickases[16,17], and dimeric fusions of catalytically inactive SpCas9 to a non-specific FokI nuclease[18–20]. However, these approaches are only partially effective, have as-yet unproven efficacies on a genome-wide scale, and/or possess the potential to create more new off-target sites. Furthermore, some require expression of multiple sgRNAs and/or fusion of additional functional domains to Cas9, which can reduce targeting range and create challenges for delivery with viral vectors that have limits on nucleic acid payload size. Thus, a major challenge for the field remains the development of a robust and easily used strategy that eliminates off-target mutations on a genome-wide scale.

We initially hypothesized that off-target effects of SpCas9 might be minimized by decreasing non-specific interactions with its target DNA site. SpCas9–sgRNA complexes cleave target sites composed of an NGG protospacer adjacent motif (PAM) sequence (recognized by SpCas9)[21–24] and an adjacent 20 base pair (bp) protospacer sequence (which is complementary to the 5′ end of the sgRNA)[22,25–27]. We previously proposed that the SpCas9–sgRNA complex might possess more energy than is needed for optimal recognition of its intended target DNA site, thereby enabling cleavage of mismatched off-target sites[14]. Structural studies have suggested that the SpCas9–sgRNA-target DNA complex encompasses several SpCas9-mediated DNA contacts, including direct hydrogen bonds made by four SpCas9 residues (N497, R661, Q695, Q926) to the phosphate backbone of the target DNA strand[28,29] (Fig. 1a and Extended Data Fig. 1a, b). We envisioned that disruption of one or more of these contacts might alter the energetics of the SpCas9–sgRNA complex so that it might retain enough for robust on-target activity but have a diminished ability to cleave mismatched off-target sites.

## Alteration of SpCas9 DNA contacts

Guided by this excess energy hypothesis, we first constructed 15 different SpCas9 variants bearing all possible single, double, triple, and quadruple combinations of N497A, R661A, Q695A, and Q926A substitutions to test whether contacts made by these residues might be dispensable for on-target activity (Fig. 1b). For these experiments, we used a previously described human cell-based enhanced GFP (EGFP) disruption assay[30]. Using an *EGFP*-targeted sgRNA, which we have previously shown can efficiently induce insertion or deletion mutations (indels) in an *EGFP* reporter gene when paired with wild-type SpCas9 (ref. 4), we found that all 15 SpCas9 variants possessed activities comparable to that of wild-type SpCas9 (Fig. 1b, grey bars). Thus, alanine substitution of one or all of these residues did not reduce on-target cleavage efficiency of SpCas9 with this *EGFP*-targeted sgRNA.

Next, we sought to assess the relative activities of all 15 SpCas9 variants at mismatched target sites. To do this, we repeated the EGFP disruption assay with derivatives of the *EGFP*-targeted sgRNA used in the previous experiment that contain pairs of substituted bases at positions ranging from 13 to 19 (numbering starting with 1 for the most PAM-proximal base and ending with 20 for the most PAM-distal base; Fig. 1b). This analysis revealed that one of the triply substituted variants (R661A/Q695A/Q926A) and the quadruple substitution variant (N497A/R661A/Q695A/Q926A) both showed minimal EGFP disruption at or near background levels with all four of the mismatched

[1]Molecular Pathology Unit, Center for Cancer Research, and Center for Computational and Integrative Biology, Massachusetts General Hospital, Charlestown, Massachusetts 02129, USA. [2]Department of Pathology, Harvard Medical School, Boston, Massachusetts 02115, USA. [3]Department of Biomedical Sciences, City University of Hong Kong, Hong Kong, China.
*These authors contributed equally to this work.

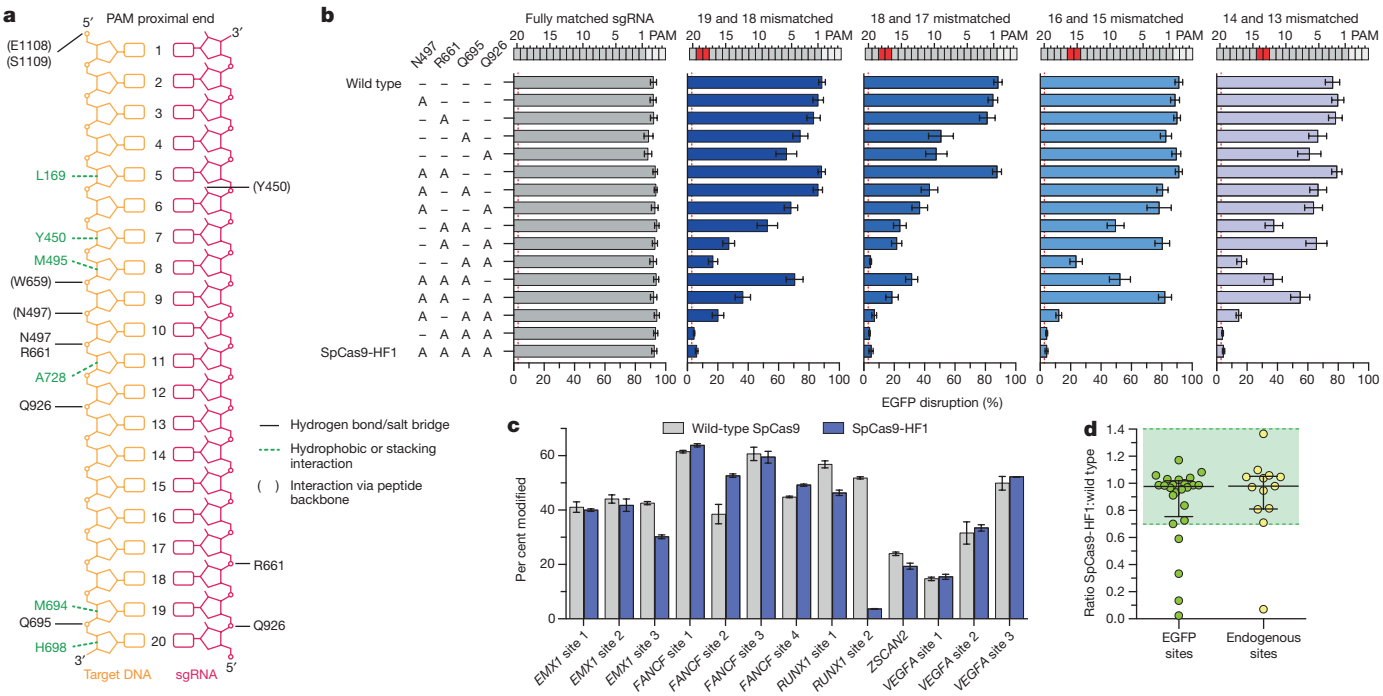


**Figure 1 | Identification and characterization of SpCas9 variants bearing substitutions in residues that form non-specific DNA contacts.** **a**, Schematic depicting wild-type SpCas9 interactions with the target DNA–sgRNA duplex, based on PDB accession 4OO8 and 4UN3 (adapted from refs 28 and 29, respectively). **b**, Characterization of SpCas9 variants that contain alanine substitutions in positions that form hydrogen bonds with the DNA backbone. Wild-type SpCas9 and variants were assessed using the human cell EGFP disruption assay when programmed with a perfectly matched sgRNA or partially mismatched sgRNAs. Error bars represent s.e.m. for $n = 3$; mean level of background EGFP loss represented by red dashed line. **c**, On-target activities of wild-type SpCas9 and SpCas9-HF1 across 13 endogenous sites measured by T7 endonuclease I assay. Error bars represent s.e.m. for $n = 3$. **d**, Ratio of on-target activity of SpCas9-HF1 to wild-type SpCas9. The median and interquartile range are shown; the interval with >70% of wild-type activity is highlighted in green.

sgRNAs (Fig. 1b, coloured bars). Based on these results, we chose the quadruple substitution variant (hereafter referred to as SpCas9-HF1 for high-fidelity variant number 1) for further analysis.

## SpCas9-HF1 retains high on-target activities

To determine how robustly SpCas9-HF1 functions at a larger number of on-target sites, we performed direct comparisons between this variant and wild-type SpCas9 using additional sgRNAs. In total, we tested 37 different sgRNAs, 24 targeted to *EGFP* and 13 targeted to endogenous human gene targets. For 20 of the 24 sgRNAs tested using the EGFP disruption assay (Extended Data Fig. 2a) and 12 of the 13 sgRNAs tested using a T7 endonuclease I mismatch assay (Fig. 1c), we found SpCas9-HF1 exhibited at least 70% of the on-target activities observed with wild-type SpCas9 at the same sites (Fig. 1d). Indeed, SpCas9-HF1 showed highly comparable activities (90–140%) to wild-type SpCas9 with the vast majority of sgRNAs (Fig. 1d). Three of the 37 sgRNAs tested showed essentially no activity with SpCas9-HF1 *(EGFP* sites 9 and 23, and *RUNX1* site 2), and examination of these target sites did not suggest any obvious differences in the characteristics of these sequences compared to those for which we saw high activities (Supplementary Table 1). Overall, SpCas9-HF1 possesses comparable activities (greater than 70% of wild-type SpCas9 activities) for 86% (32/37) of the sgRNAs we tested.

## Genome-wide specificity of SpCas9-HF1

To test whether SpCas9-HF1 exhibits reduced off-target effects in human cells, we used the genome-wide unbiased identification of double-stranded breaks enabled by sequencing (GUIDE-seq) method[8] to assess eight different sgRNAs targeted to sites in the endogenous human *EMX1*, *FANCF*, *RUNX1*, and *ZSCAN2* genes. The sequences targeted by these sgRNAs have variable numbers of predicted mismatched sites in the reference human genome (Extended Data Table 1). Assessment of on-target double-stranded oligodeoxynucleotide (dsODN) tag integration (by restriction-fragment length polymorphism (RFLP) assay) and indel formation (by T7 endonuclease I assay) for the eight sgRNAs revealed comparable on-target activities with wild-type SpCas9 and SpCas9-HF1 (Extended Data Fig. 3a and 3b, respectively), demonstrating that these GUIDE-seq experiments were working efficiently and comparably with the two different nucleases.

These GUIDE-seq experiments showed that with wild-type SpCas9, seven of the eight sgRNAs induced cleavage at multiple off-target sites (ranging from 2 to 25 per sgRNA), whereas the eighth sgRNA (*FANCF* site 4) did not yield any detectable off-target sites (Fig. 2a, b). The off-target sites identified harboured one to six mismatches distributed throughout various positions in the protospacer and/or PAM sequence (Fig. 2c and Extended Data Fig. 4a). However, with SpCas9-HF1, a complete absence of GUIDE-seq detectable off-target events was observed for six of the seven sgRNAs that induced off-target effects with wild-type SpCas9 (Fig. 2a, b). Among these seven sgRNAs, only a single detectable genome-wide off-target was identified, for *FANCF* site 2, at a site harbouring one mismatch within the protospacer seed sequence (Fig. 2a). As with wild-type SpCas9, the eighth sgRNA (*FANCF* site 4) did not yield any detectable off-target cleavage events when tested with SpCas9-HF1 (Fig. 2a). Notably, with all eight sgRNAs, SpCas9-HF1 did not create any new nuclease-induced off-target sites (not already observed with wild-type SpCas9) detectable by GUIDE-seq.

To confirm these GUIDE-seq findings, we used targeted amplicon sequencing to more directly measure the frequencies of indel mutations induced by wild-type SpCas9 and SpCas9-HF1. For these experiments, we transfected human cells only with sgRNA- and Cas9-encoding plasmids (without the GUIDE-seq tag). We used next-generation sequencing to examine the on-target sites and 36 of the 40 off-target sites that had been identified for six sgRNAs with wild-type

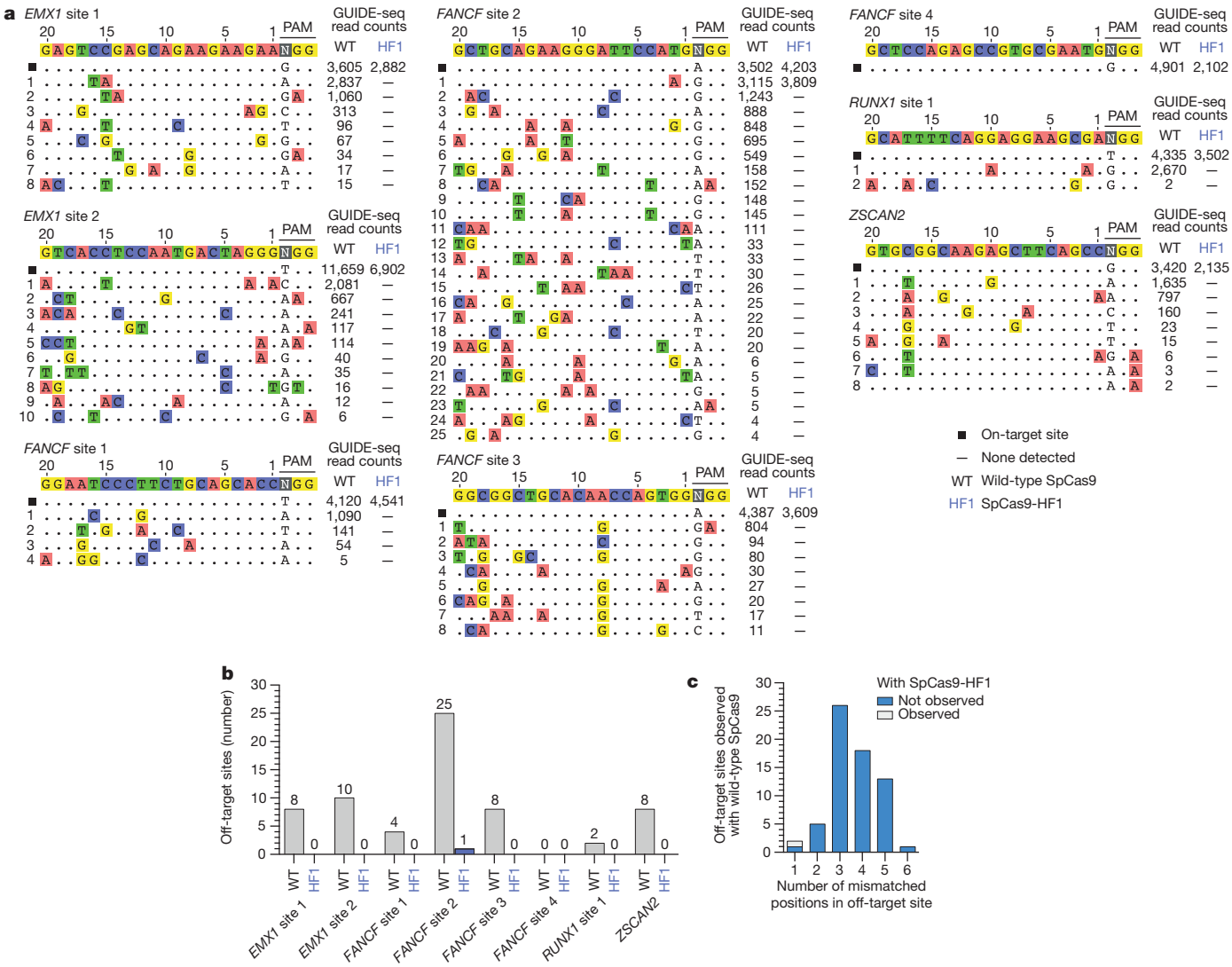


**Figure 2 | Genome-wide specificities of wild-type SpCas9 and SpCas9-HF1 with sgRNAs targeted to standard, non-repetitive sites.** **a**, Off-target cleavage sites of wild-type SpCas9 and SpCas9-HF1 with eight sgRNAs targeted to endogenous human genes, as determined by GUIDE-seq. Read counts represent a measure of cleavage frequency at a given site; mismatched positions within the spacer or PAM are highlighted in colour. **b**, Summary of the total number of genome-wide off-target sites identified by GUIDE-seq for wild-type SpCas9 and SpCas9-HF1 with the sgRNAs used in panel **a**. **c**, Off-target sites identified for wild-type SpCas9 and SpCas9-HF1 for the eight sgRNAs, binned according to the total number of mismatches (in the protospacer and PAM) relative to the on-target site.

SpCas9 in our GUIDE-seq experiments (four of the 40 sites could not be specifically amplified from genomic DNA). These deep sequencing experiments showed that: (1) wild-type SpCas9 and SpCas9-HF1 induced comparable frequencies of indels at each of the six sgRNA on-target sites, indicating that the nucleases and sgRNAs were functional in all experimental replicates (Fig. 3a, b); (2) as expected, wild-type SpCas9 showed statistically significant evidence of indel mutations at 35 of the 36 off-target sites (Fig. 3b) at frequencies that correlated well with GUIDE-seq read counts for these same sites (Fig. 3c); and (3) the frequencies of indels induced by SpCas9-HF1 at 34 of the 36 off-target sites were statistically indistinguishable from the background level of indels observed in samples from control transfections (Fig. 3b). For the two off-target sites that appeared to have statistically significant mutation frequencies with SpCas9-HF1 relative to the negative control, the mean frequencies of indels were 0.049% and 0.037%, levels at which it is difficult to determine whether these are due to sequencing or PCR error or are bona fide nuclease-induced indels. Based on these results, we conclude that SpCas9-HF1 can completely or nearly completely reduce off-target mutations that occur across a range of different frequencies with wild-type SpCas9 to levels generally undetectable by GUIDE-seq and targeted deep sequencing.

We next assessed the capability of SpCas9-HF1 to reduce genome-wide off-target effects of sgRNAs designed against atypical homopolymeric or repetitive sequences. Although we and other researchers now try to avoid on-target sites with these characteristics due to their relative lack of orthogonality to the genome, we wished to challenge the genome-wide specificity of SpCas9-HF1 with sites that have very large numbers of known off-target sites in human cells. Therefore, we used previously characterized sgRNAs[4,8] that target either a cytosine-rich homopolymeric sequence or a sequence containing multiple TG repeats in the human *VEGFA* gene (*VEGFA* site 2 and *VEGFA* site 3, respectively) (Extended Data Table 1). In control experiments, we again found that each of these sgRNAs induced comparable levels of GUIDE-seq dsODN tag incorporation (Extended Data Fig. 3c) and indel mutations (Extended Data Fig. 3d) with both wild-type SpCas9 and SpCas9-HF1, demonstrating that SpCas9-HF1 is not impaired in on-target activity with either of these sgRNAs. Importantly, these GUIDE-seq experiments revealed that SpCas9-HF1 was highly effective at reducing off-target sites of these sgRNAs, with 123/144 sites for *VEGFA* site 2 and 31/32 sites for *VEGFA* site 3 not detected (Fig. 4a and Extended Data Fig. 5). Examination of wild-type SpCas9 off-target sites not detected with SpCas9-HF1 showed that they each possessed a

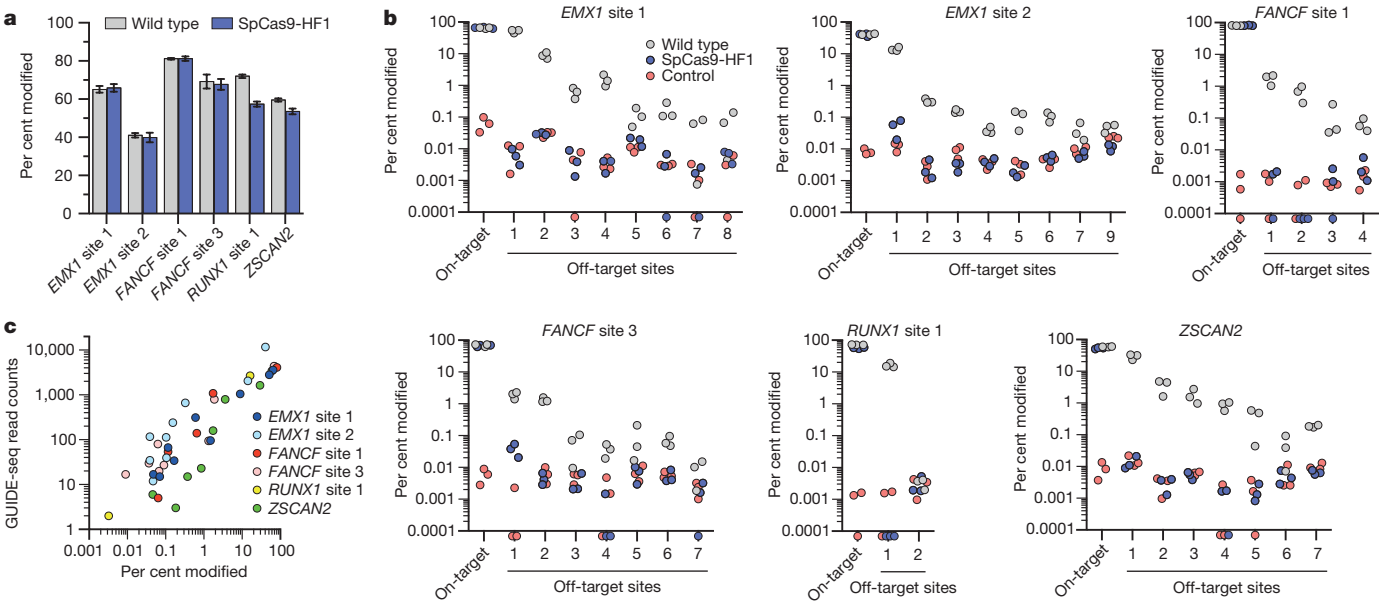


**Figure 3 | Validation of SpCas9-HF1 specificity improvements by deep sequencing of off-target sites identified by GUIDE-seq. a**, Mean on-target per cent modification for wild-type SpCas9 and SpCas9-HF1 with six sgRNAs from Fig. 2. Error bars represent s.e.m. for $n = 3$. **b**, Per cent modification of on-target and GUIDE-seq detected off-target sites with indel mutations. Triplicate experiments are plotted for wild-type SpCas9, SpCas9-HF1, and a negative control; off-target sites are numbered as indicated in Fig. 2a. Filled circles below the *x* axis represent replicates for which no indels were observed (Supplementary Table 4). Hypothesis testing using a one-sided Fisher exact test with pooled read counts found significant differences ($P < 0.05$ after adjusting for multiple comparisons using the Benjamini–Hochberg method) for comparisons between SpCas9-HF1 and the control condition only at *EMX1* site 2 off-target 1 and *FANCF* site 3 off-target 1. Significant differences were also found between wild-type SpCas9 and SpCas9-HF1 at all off-target sites, and between wild-type SpCas9 and the control condition at all off-target sites except *RUNX1* site 1 off-target 2. **c**, Scatter plot of the correlation between GUIDE-seq read counts (from Fig. 2a) and mean per cent modification determined by deep sequencing at on- and off-target cleavage sites with wild-type SpCas9.

range of total mismatches distributed at various positions within their protospacer and PAM sequences: 2 to 7 mismatches for the *VEGFA* site 2 sgRNA and 1 to 4 mismatches for the *VEGFA* site 3 sgRNA (Fig. 4b and Extended Data Fig. 4b); also, nine of these off-targets for *VEGFA* site 2 may be recognized by an alternate potential base pairing interaction with the sgRNA that might occur with a single bulged base[12] at the sgRNA–DNA interface (Extended Data Figs 5 and 6). Overall, the sites that were still mutated by SpCas9-HF1 possessed a range of 2 to 6 mismatches for the *VEGFA* site 2 sgRNA and 2 mismatches in the single site for the *VEGFA* site 3 sgRNA (Fig. 4b), with three of the off-target sites for the *VEGFA* site 2 sgRNA having an alternative potential single bulge alignment (Extended Data Figs 5 and 6). Notably, no new nuclease-induced off-target sites were induced by SpCas9-HF1 with either of the two sgRNAs. Collectively, these results demonstrate that SpCas9-HF1 can be highly effective at reducing off-target effects of sgRNAs targeted to simple repeat sequences and can also have substantial impacts on sgRNAs targeted to homopolymeric sequences.

## Refining the specificity of SpCas9–HF1

Previously described methods such as truncated sgRNAs[14] and the SpCas9 D1135E variant[15] can partially reduce SpCas9 off-target effects, and we therefore wondered whether these might be combined with SpCas9-HF1 to further improve its genome-wide specificity. Testing of SpCas9-HF1 with matched full-length and truncated sgRNAs targeted to four sites in the human cell-based EGFP disruption assay revealed that shortening sgRNA complementarity length substantially impaired on-target activities (Extended Data Fig. 7a). By contrast, SpCas9-HF1 with an additional D1135E substitution (a variant we call SpCas9-HF2) retained 70% or more activity of wild-type SpCas9 with six of eight sgRNAs tested using our human cell-based EGFP disruption assay (Fig. 5a and Extended Data Fig. 2b). We also constructed SpCas9-HF3 and SpCas9-HF4 variants harbouring additional L169A or Y450A substitutions, respectively, at positions whose side chains are believed to mediate non-specific hydrophobic interactions with the target DNA on its PAM proximal end[28,31] (Fig. 1a). The Y450 residue is notable for participating in a base stacking interaction with the sgRNA[31] and undergoing a 120 degree shift upon target binding to create its hydrophobic interaction with the DNA[28,32]. SpCas9-HF3 and SpCas9-HF4 retained 70% or more of the activities observed with wild-type SpCas9 with the same six out of eight *EGFP*-targeted sgRNAs (Fig. 5a and Extended Data Fig. 2b).

We next sought to determine whether SpCas9-HF2, -HF3, or -HF4 could reduce indel frequencies at two off-target sites that remained susceptible to modification by SpCas9-HF1, one with the *FANCF* site 2 sgRNA and another with the *VEGFA* site 3 sgRNA. For the *FANCF* site 2 off-target, which bears a single mismatch in the seed sequence of the protospacer, we found that SpCas9-HF4 (containing the additional Y450A substitution) reduced indel mutation frequencies to near background level as judged by T7 endonuclease I assay, while also beneficially

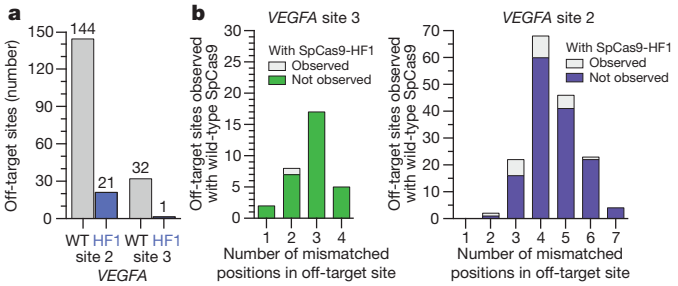


**Figure 4 | Genome-wide specificities of wild-type SpCas9 and SpCas9-HF1 with sgRNAs targeted to non-standard, repetitive sites.** **a**, Summary of the total number of genome-wide off-target cleavage sites identified by GUIDE-seq for wild-type SpCas9 and SpCas9-HF1 with sgRNAs targeted to *VEGFA* sites 2 and 3. **b**, Off-target sites identified for wild-type SpCas9 or SpCas9-HF1 with sgRNAs targeted to *VEGFA* sites 2 and 3 binned according to the total number of mismatches (within the protospacer and PAM) relative to the on-target site.

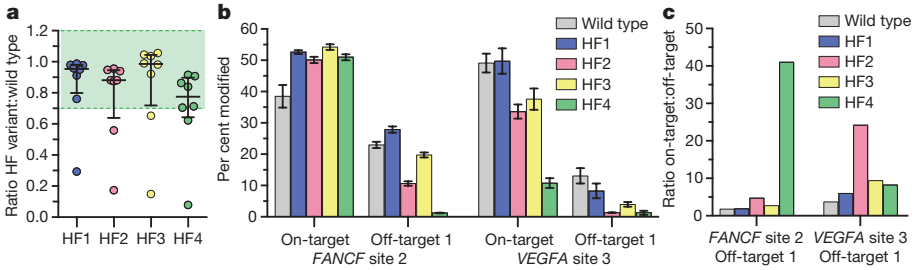


**Figure 5 | Activities of high-fidelity derivatives of SpCas9-HF1 bearing additional substitutions. a**, Summary of the on-target EGFP disruption activities of various SpCas9-HF variants compared to wild-type SpCas9 (from the data in Extended Data Fig. 2b). SpCas9-HF1 contains N497A, R661A, Q695A, and Q926A substitutions; HF2 = HF1 + D1135E; HF3 = HF1 + L169A; HF4 = HF1 + Y450A. The median and interquartile range are shown; the interval showing >70% of wild-type activity is highlighted in green. **b**, Mean per cent modification by SpCas9 and HF variants at the *FANCF* site 2 and *VEGFA* site 3 on-target sites, as well as off-target sites from Fig. 2a and Extended Data Fig. 5 resistant to the effects of SpCas9-HF1. Per cent modification determined by T7 endonuclease I assay; background indel percentages were subtracted for all experiments; error bars represent s.e.m. for $n = 3$. **c**, Specificity ratios of wild-type SpCas9 and HF variants with the *FANCF* site 2 or *VEGFA* site 3 sgRNAs, plotted as the ratio of on-target to off-target activity (from panel **b**).

increasing on-target activity (Fig. 5b), resulting in the greatest increase in specificity among the three variants (Fig. 5c). For the *VEGFA* site 3 off-target site, which bears two protospacer mismatches (one in the seed sequence and one at the nucleotide most distal from the PAM sequence), SpCas9-HF2 (containing the additional D1135E substitution) showed near background levels of indel formation as determined by T7 endonuclease I assay while showing modest effects on on-target mutation efficiency (Fig. 5b), leading to the greatest increase in specificity for this off-target site among the three variants tested (Fig. 5c).

## Discussion

The SpCas9-HF1 variant characterized in this report reduces all or nearly all genome-wide off-target effects to undetectable levels as judged by GUIDE-seq and targeted next-generation sequencing, with the most robust and consistent effects observed with sgRNAs designed against standard, non-repetitive target sequences. Our observations suggest that off-target mutations might be minimized by using SpCas9-HF1 to target non-repetitive sequences that do not have closely matched sites (for example, bearing 1 or 2 mismatches) elsewhere in the genome; such sites can be easily identified using existing publicly available software programs[33]. An interesting question will be to determine whether SpCas9-HF1 induces off-target mutations at frequencies below the detection limit of existing unbiased genome-wide methods (Supplementary Discussion). We also discuss other practical considerations for targeting sites of interest with SpCas9-HF1, including the use of sgRNAs with non-G or mismatched 5′ nucleotides (Extended Data Fig. 7b) and altering the PAM recognition specificity of SpCas9-HF1 (Extended Data Fig. 8), in the Supplementary Discussion.

Further biochemical experiments and structural characterization will be required to define the mechanism by which SpCas9-HF1 achieves its high genome-wide specificity. We do not believe that the four substitutions we introduced alter the stability or steady-state expression level of SpCas9 in human cells, because titration experiments with decreasing concentrations of expression plasmids suggest that wild-type SpCas9 and SpCas9-HF1 behave comparably as their amounts are lowered (Extended Data Fig. 9). Although our initial rationale for making the substitutions in SpCas9-HF1 was to decrease the energetics of interaction between the Cas9-sgRNA complex and the target DNA (as has been previously proposed to explain the increased specificities of transcription activator-like effector nucleases bearing substitutions at positively charged residues[34]), recent work has provided greater mechanistic insights into SpCas9 recognition and cleavage. These studies suggest alternative and more detailed models (for example, formation of an active cleavage complex through conformational changes or kinetics of off-target site recognition[35,36] that might be affected by the substitutions in our SpCas9-HF1 variant (Supplementary Discussion)).

More broadly, our results validate a general strategy for the engineering of additional high-fidelity variants of CRISPR-associated nucleases. We found that introducing substitutions at other non-specific DNA contacting residues can further reduce some of the very small number of residual off-target sites that persist for certain sgRNAs with SpCas9-HF1. Thus, we envision that variants such as SpCas9-HF2, SpCas9-HF4, and others might be used in a customized fashion to eliminate any potential off-target sites that might be resistant to the specificity improvements of SpCas9-HF1. In addition, our variants might be combined with substitutions in residues that contact the non-target DNA strand, alterations that have been shown to reduce SpCas9 off-target effects while our manuscript was under review[37]. Overall, our results demonstrate that the approach of mutating non-specific DNA contacts is highly effective at increasing SpCas9 specificity and suggest it might be extended to other naturally occurring and engineered Cas9 orthologues[38–42], as well as other CRISPR-associated nucleases[43,44].

**Online Content** Methods, along with any additional Extended Data display items and Source Data, are available in the online version of the paper; references unique to these sections appear only in the online paper.

**Received 8 November; accepted 9 December 2015.**
**Published online 6 January 2016.**

1. Hsu, P. D., Lander, E. S. & Zhang, F. Development and applications of CRISPR–Cas9 for genome engineering. *Cell* **157,** 1262–1278 (2014).
2. Sander, J. D. & Joung, J. K. CRISPR–Cas systems for editing, regulating and targeting genomes. *Nature Biotechnol.* **32,** 347–355 (2014).
3. Doudna, J. A. & Charpentier, E. Genome editing. The new frontier of genome engineering with CRISPR–Cas9. *Science* **346,** 1258096 (2014).
4. Fu, Y. *et al.* High-frequency off-target mutagenesis induced by CRISPR–Cas nucleases in human cells. *Nature Biotechnol.* **31,** 822–826 (2013).
5. Hsu, P. D. *et al.* DNA targeting specificity of RNA-guided Cas9 nucleases. *Nature Biotechnol.* **31,** 827–832 (2013).
6. Pattanayak, V. *et al.* High-throughput profiling of off-target DNA cleavage reveals RNA-programmed Cas9 nuclease specificity. *Nature Biotechnol.* **31,** 839–843 (2013).
7. Cradick, T. J., Fine, E. J., Antico, C. J. & Bao, G. CRISPR/Cas9 systems targeting β-globin and *CCR5* genes have substantial off-target activity. *Nucleic Acids Res.* **41,** 9584–9592 (2013).
8. Tsai, S. Q. *et al.* GUIDE-seq enables genome-wide profiling of off-target cleavage by CRISPR–Cas nucleases. *Nature Biotechnol.* **33,** 187–197 (2015).
9. Frock, R. L. *et al.* Genome-wide detection of DNA double-stranded breaks induced by engineered nucleases. *Nature Biotechnol.* **33,** 179–186 (2015).
10. Wang, X. *et al.* Unbiased detection of off-target cleavage by CRISPR–Cas9 and TALENs using integrase-defective lentiviral vectors. *Nature Biotechnol.* **33,** 175–178 (2015).
11. Kim, D. *et al.* Digenome-seq: genome-wide profiling of CRISPR–Cas9 off-target effects in human cells. *Nature Methods* **12,** 237–243 (2015).
12. Lin, Y. *et al.* CRISPR/Cas9 systems have off-target activity with insertions or deletions between target DNA and guide RNA sequences. *Nucleic Acids Res.* **42,** 7473–7485 (2014).
13. Cho, S. W. *et al.* Analysis of off-target effects of CRISPR/Cas-derived RNA-guided endonucleases and nickases. *Genome Res.* **24,** 132–141 (2014).
14. Fu, Y., Sander, J. D., Reyon, D., Cascio, V. M. & Joung, J. K. Improving CRISPR–Cas nuclease specificity using truncated guide RNAs. *Nature Biotechnol.* **32,** 279–284 (2014).

15. Kleinstiver, B. P. *et al.* Engineered CRISPR–Cas9 nucleases with altered specificities. *Nature* **523,** 481–485 (2015).
16. Mali, P. *et al.* CAS9 transcriptional activators for target specificity screening and paired nickases for cooperative genome engineering. *Nature Biotechnol.* **31,** 833–838 (2013).
17. Ran, F. A. *et al.* Double nicking by RNA-guided CRISPR Cas9 for enhanced genome editing specificity. *Cell* **154,** 1380–1389 (2013).
18. Tsai, S. Q. *et al.* Dimeric CRISPR RNA-guided FokI nucleases for highly specific genome editing. *Nature Biotechnol.* **32,** 569–576 (2014).
19. Guilinger, J. P., Thompson, D. B. & Liu, D. R. Fusion of catalytically inactive Cas9 to FokI nuclease improves the specificity of genome modification. *Nature Biotechnol.* **32,** 577–582 (2014).
20. Wyvekens, N., Topkar, V. V., Khayter, C., Joung, J. K. & Tsai, S. Q. Dimeric CRISPR RNA-guided FokI-dCas9 nucleases directed by truncated gRNAs for highly specific genome editing. *Hum. Gene Ther.* **26,** 425–431 (2015).
21. Deltcheva, E. *et al.* CRISPR RNA maturation by *trans*-encoded small RNA and host factor RNase III. *Nature* **471,** 602–607 (2011).
22. Jinek, M. *et al.* A programmable dual-RNA-guided DNA endonuclease in adaptive bacterial immunity. *Science* **337,** 816–821 (2012).
23. Jiang, W., Bikard, D., Cox, D., Zhang, F. & Marraffini, L. A. RNA-guided editing of bacterial genomes using CRISPR–Cas systems. *Nature Biotechnol.* **31,** 233–239 (2013).
24. Sternberg, S. H., Redding, S., Jinek, M., Greene, E. C. & Doudna, J. A. DNA interrogation by the CRISPR RNA-guided endonuclease Cas9. *Nature* **507,** 62–67 (2014).
25. Jinek, M. *et al.* RNA-programmed genome editing in human cells. *Elife* **2,** e00471 (2013).
26. Mali, P. *et al.* RNA-guided human genome engineering via Cas9. *Science* **339,** 823–826 (2013).
27. Cong, L. *et al.* Multiplex genome engineering using CRISPR/Cas systems. *Science* **339,** 819–823 (2013).
28. Nishimasu, H. *et al.* Crystal structure of Cas9 in complex with guide RNA and target DNA. *Cell* **156,** 935–949 (2014).
29. Anders, C., Niewoehner, O., Duerst, A. & Jinek, M. Structural basis of PAM-dependent target DNA recognition by the Cas9 endonuclease. *Nature* **513,** 569–573 (2014).
30. Reyon, D. *et al.* FLASH assembly of TALENs for high-throughput genome editing. *Nature Biotechnol.* **30,** 460–465 (2012).
31. Jiang, F., Zhou, K., Ma, L., Gressel, S. & Doudna, J. A. A Cas9-guide RNA complex preorganized for target DNA recognition. *Science* **348,** 1477–1481 (2015).
32. Jinek, M. *et al.* Structures of Cas9 endonucleases reveal RNA-mediated conformational activation. *Science* **343,** http://dx.doi.org/10.1126/science.1247997 (2014).
33. Bae, S., Park, J. & Kim, J. S. Cas-OFFinder: a fast and versatile algorithm that searches for potential off-target sites of Cas9 RNA-guided endonucleases. *Bioinformatics* **30,** 1473–1475 (2014).
34. Guilinger, J. P. *et al.* Broad specificity profiling of TALENs results in engineered nucleases with improved DNA-cleavage specificity. *Nature Methods* **11,** 429–435 (2014).
35. Sternberg, S. H., LaFrance, B., Kaplan, M. & Doudna, J. A. Conformational control of DNA target cleavage by CRISPR–Cas9. *Nature* **527,** 110–113 (2015).
36. Knight, S. C. *et al.* Dynamics of CRISPR–Cas9 genome interrogation in living cells. *Science* **350,** 823–826 (2015).
37. Slaymaker, I. M. *et al.* Rationally engineered Cas9 nucleases with improved specificity. *Science* http://dx.doi.org/10.1126/science.aad5227 (2015).
38. Ran, F. A. *et al. In vivo* genome editing using *Staphylococcus aureus* Cas9. *Nature* **520,** 186–191 (2015).
39. Esvelt, K. M. *et al.* Orthogonal Cas9 proteins for RNA-guided gene regulation and editing. *Nature Methods* **10,** 1116–1121 (2013).
40. Hou, Z. *et al.* Efficient genome engineering in human pluripotent stem cells using Cas9 from *Neisseria meningitidis*. *Proc. Natl Acad. Sci. USA* **110,** 15644–15649 (2013).
41. Fonfara, I. *et al.* Phylogeny of Cas9 determines functional exchangeability of dual-RNA and Cas9 among orthologous type II CRISPR–Cas systems. *Nucleic Acids Res.* **42,** 2577–2590 (2014).
42. Kleinstiver, B. P. *et al.* Broadening the targeting range of *Staphylococcus aureus* CRISPR–Cas9 by modifying PAM recognition. *Nature Biotechnol.* **33,** 1293–1298 (2015).
43. Zetsche, B. *et al.* Cpf1 is a single RNA-Guided endonuclease of a class 2 CRISPR–Cas system. *Cell* **163,** 759–771 (2015).
44. Shmakov, S. *et al.* Discovery and functional characterization of diverse class 2 CRISPR–Cas systems. *Mol. Cell* **60,** 385–397 (2015).


**Supplementary Information** is available in the online version of the paper.

**Acknowledgements** B.P.K. is supported by a Natural Sciences and Engineering Research Council of Canada Postdoctoral Fellowship. V.P. was supported by the Massachusetts General Hospital (MGH) Department of Pathology. S.Q.T. is supported by an MGH Tosteson and Fund for Medical Discovery Fellowship. J.K.J. is supported by a US National Institutes of Health (NIH) Director's Pioneer Award (DP1 GM105378), NIH R01 GM107427, NIH R01 GM088040, and the Jim and Ann Orr MGH Research Scholar Award.

**Author Contributions** B.P.K., V.P., and J.K.J. conceived of and designed experiments. B.P.K., V.P., and M.S.P. performed all experiments. N.T.N. contributed to GUIDE-seq library preparation. B.P.K., V.P., M.S.P., S.Q.T., and Z.Z. analysed the data. B.P.K., V.P., and J.K.J. wrote the manuscript with input from all the authors.

**Author Information** Plasmids encoding the high-fidelity SpCas9, VQR, and VRQR variants described in this manuscript have been deposited with the non-profit plasmid distribution service Addgene (http://www.addgene.org/crispr-cas). All sequencing data from this study is available through the NCBI Sequence Read Archive (SRA) under accession number SRP066862. Reprints and permissions information is available at www.nature.com/reprints. The authors declare competing financial interests: details are available in the online version of the paper. Readers are welcome to comment on the online version of the paper. Correspondence and requests for materials should be addressed to J.K.J. (jjoung@mgh.harvard.edu).

## METHODS

**Data reporting.** No statistical methods were used to predetermine sample size. The investigators were not blinded to allocation during experiments and outcome assessment.

**Plasmids and oligonucleotides.** DNA sequences of plasmids used in this study can be found in the Supplementary Information. sgRNA target sites are available in Supplementary Table 1, and oligonucleotides used in this study can be found in Supplementary Table 2. SpCas9 expression plasmids containing amino acid substitutions were generated by standard PCR and molecular cloning into JDS246 (ref. 4). sgRNA expression plasmids were constructed by ligating oligonucleotide duplexes into BsmBI cut BPK1520 (ref. 15). Unless otherwise indicated, all sgRNAs were designed to target sites containing a 5′ guanine nucleotide.

**Human cell culture and transfection.** U2OS cells (a gift from Toni Cathomen, Freiburg) and U2OS.EGFP cells (containing a single integrated copy of a reporter gene encoding an EGFP–PEST fusion)[30] were cultured in advanced DMEM supplemented with 10% heat-inactivated fetal bovine serum, 2 mM GlutaMax, and penicillin and streptomycin at 37 °C with 5% $CO_2$. The growth media for U2OS.EGFP cells was additionally supplemented with 400 μg ml$^{-1}$ Geneticin. All cell culture reagents were obtained from Life Technologies. Cell line identity was validated by STR profiling (ATCC) and deep-sequencing, and cells were tested bi-weekly for mycoplasma contamination. Unless otherwise noted, cells were co-transfected with 750 ng of Cas9 plasmid and 250 ng of sgRNA plasmid. For negative control experiments, Cas9 plasmids were co-transfected with a U6-null plasmid. Nucleofections were performed using the DN-100 program on a Lonza 4-D Nucleofector with the SE Cell Line Kit according to the manufacturer's protocol (Lonza). For T7 endonuclease I assays, GUIDE-seq experiments, and targeted deep sequencing, genomic DNA was extracted ~72 h post-transfection using the Agencourt DNAdvance Genomic DNA Isolation Kit (Beckman Coulter Genomics).

**Human cell EGFP disruption assay.** EGFP disruption experiments, in which cleavage and induction of indels by non-homologous end-joining (NHEJ)-mediated repair within a single integrated *EGFP* reporter gene leads to loss of cell fluorescence, were performed as previously described[4,30]. Briefly, transfected cells were analysed ~52 h post-transfection for loss of EGFP expression using a Fortessa flow cytometer (BD Biosciences). Background EGFP loss was determined using negative control transfections gated at ~2.5% for all experiments (represented as a red dashed line in figures). *P* values for comparisons between SpCas9 variants were calculated using a one-sided *t*-test with equal variances and adjusted for multiple comparisons using the method of Benjamini and Hochberg (Supplementary Table 3).

**T7 endonuclease I assays.** To quantify mutagenesis frequencies at desired genomic loci, T7 endonuclease I assays were performed as previously described[30]. Briefly, on- or off-target sites were amplified from ~100 ng of genomic DNA using Phusion Hot-Start Flex DNA Polymerase (New England Biolabs) using the primers listed in Supplementary Table 2. An Agencourt Ampure XP cleanup (Beckman Coulter Genomics) was performed before the denaturation and annealing of ~200 ng of the PCR product, followed by digestion with T7 endonuclease I (New England Biolabs). Purified digestion products were quantified using a QIAxcel capillary electrophoresis instrument (Qiagen) to approximate the mutagenesis frequencies induced by Cas9-sgRNA complexes. *P* values for comparisons between SpCas9 variants were calculated using a one-sided *t*-test with equal variances and adjusted for multiple comparisons using the method of Benjamini and Hochberg (Supplementary Table 3).

**GUIDE-seq.** GUIDE-seq relies on the integration of a short dsODN tag into DNA breaks to enable amplification and sequencing of adjacent genomic sequence, with the number of tag integrations at any given site providing a quantitative measure of cleavage efficiency[8]. GUIDE-seq experiments were performed and analysed essentially as previously described[8]. Briefly, U2OS cells were transfected with 750 ng of Cas9 and 250 ng sgRNA plasmids as described above, along with 100 pmol of a GUIDE-seq end-protected dsODN that contains an NdeI restriction site[8]. Restriction-fragment length polymorphism (RFLP) assays were used to estimate GUIDE-seq tag integration frequencies at the intended on-target sites as previously described[15], using the primers listed in Supplementary Table 2. The overall on-target mutagenesis frequencies of GUIDE-seq tag-treated samples was determined by T7 endonuclease I assay as described above. Tag-specific amplification and library preparation[8] were performed before high-throughput sequencing on an Illumina MiSeq instrument. GUIDE-seq data was analysed as previously described[8] using open-source GUIDE-seq analysis software (http://www.jounglab.org/guideseq) and the summarized results can be found in Supplementary Table 4. Genomic sites were excluded from analysis on the basis of overlap with background genomic breakpoint regions detected in any of four oligo-only control samples, overlap with previously identified Cas9–sgRNA independent breakpoints in human U2OS cells[8], or as neighbouring genomic window consolidation artefacts likely due to extensive end-resection around breakpoints (Supplementary Table 4). Potential RNA- or DNA-bulge sites[12] (Extended Data Fig. 6) were identified by sequence alignment with Geneious version 8.1.6 (http://www.geneious.com)[45]. Sequencing data was corrected for U2OS cell-type specific SNPs with the site encoding the smallest edit distance to the intended sgRNA site used as the most likely off-target (Supplementary Table 4). Differences in number of GUIDE-seq identified off-target sites between this work and previous studies[8,15] are likely due to different experimental conditions (for example, different promoters, quantity of plasmids used for transfection) and/or to sampling effects at the limit of detection of these particular experiments (Supplementary Table 4), and most likely not due to depth of sequencing which was similar between experiments.

Positional profiles generated from GUIDE-seq data (Extended Data Fig. 4) were made by weighting each nucleotide at each on/off-target site by the number of GUIDE-seq read counts. Sites containing gapped alignments relative to the human genome were not considered. Positional profiles for potential genomic off-target sites were restricted to sequences containing five or fewer mutations relative to the on-target site and to sequences containing NGG PAMs. Heat maps were generated with R 3.2.2 and the image function, with colours determined using the function colorRampPalette(c("white", "blue"))(2500).

**Targeted deep-sequencing.** Off-target sites identified by GUIDE-seq were amplified using Phusion High-Fidelity DNA polymerase (New England Biolabs) using the primers listed in Supplementary Table 2 for the genomic amplicons listed in Supplementary Table 5. PCR products were generated for each on- and off-target site from ~100 ng of genomic DNA extracted from U2OS cells. Products were generated from triplicate transfections for each of three experimental conditions: (1) control (wild-type SpCas9 + pSL695, a control plasmid that contains a U6 promoter but does not encode a functional sgRNA), (2) wild-type SpCas9 + sgRNA, and (3) SpCas9-HF1 + sgRNA. PCR products were purified with Ampure XP magnetic beads (Agencourt), normalized in concentration, and pooled into nine samples (individual triplicate experiments for each of the three conditions listed above). Illumina Tru-seq compatible deep-sequencing libraries were prepared using ~500 ng of each pooled sample using a 'with-bead' HTP library preparation kit (KAPA BioSystems), and sequenced via 150-bp paired-end sequencing on an Illumina MiSeq instrument. High-throughput sequencing data was analysed essentially as previously described[18]. Breifly, paired reads were mapped to the human genome (reference sequence GRChr37) using the bwa mem algorithm with default parameters. High-quality reads (average quality score ≥30) were analysed for the presence of two or more bp indels that overlapped to the on- or off-target sites (Supplementary Table 5). One bp indel mutations were only included if they occurred directly adjacent to the predicted cleavage site. *P* values for comparisons between control, wild-type SpCas9 + sgRNA, and SpCas9-HF1 + sgRNA (Supplementary Table 5) were obtained on pooled triplicate data using a one-sided Fisher exact test in the R 3.2.2 software package. *P* values for each set of comparisons were adjusted for multiple comparisons using the method of Benjamini and Hochberg (function p.adjust(method = "BH") in R).

**Code availability.** Scripts for GUIDE-seq analysis (v0.9) can be found at http://jounglab.org/guideseq. The scripts used for indel calling on deep sequencing data and GUIDE-seq profiles are available upon request.

45. Kearse, M. *et al.* Geneious Basic: an integrated and extendable desktop software platform for the organization and analysis of sequence data. *Bioinformatics* **28,** 1647–1649 (2012).

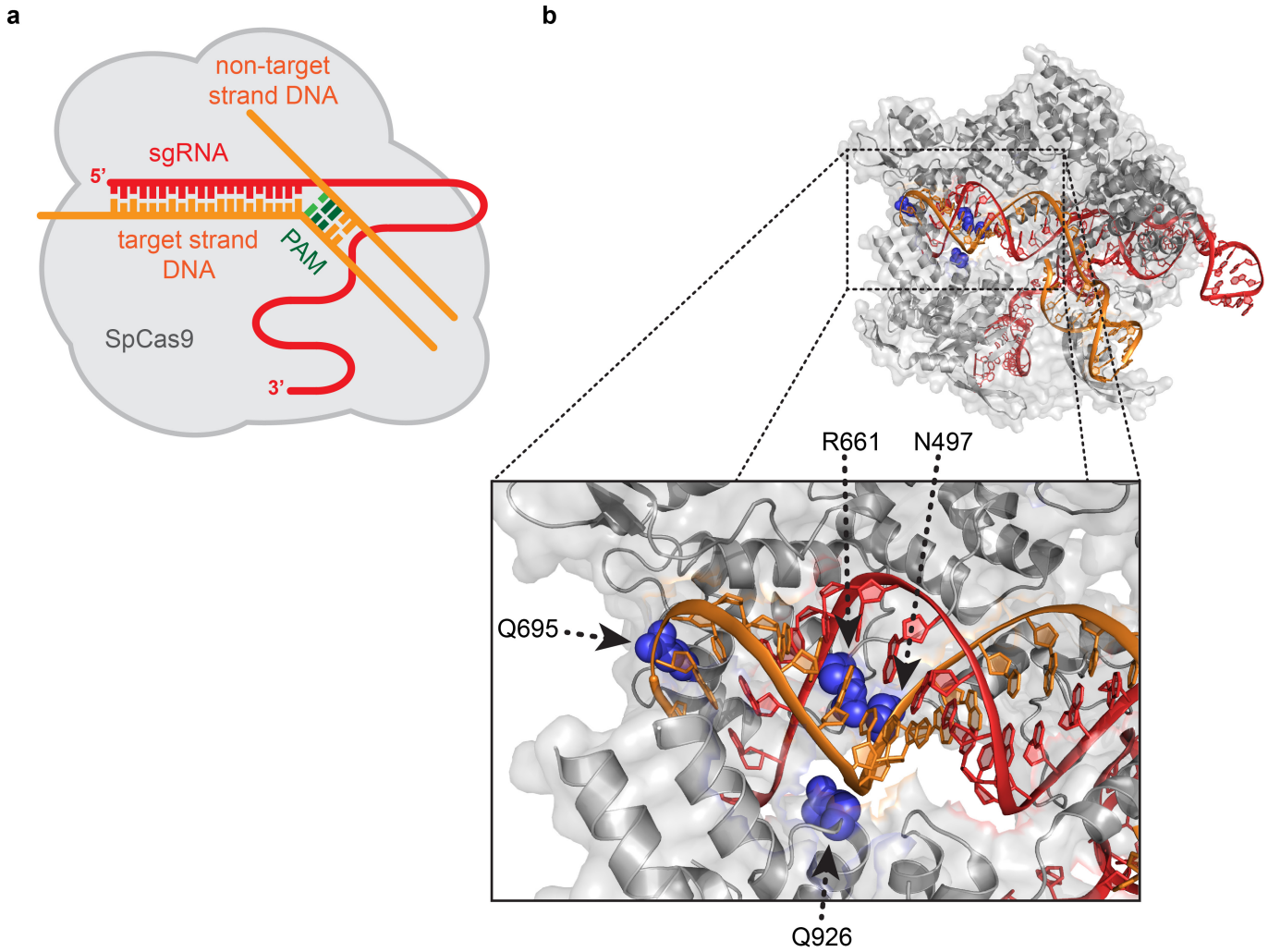


**Extended Data Figure 1 | SpCas9 interaction with the sgRNA and target DNA. a**, Schematic illustrating the SpCas9–sgRNA complex, with base pairing between the sgRNA and target DNA. **b**, Structural representation of the SpCas9-sgRNA complex bound to the target DNA, from PDB accession code 4UN3 (ref. 29). The four residues that form hydrogen bond contacts to the target-strand DNA backbone are highlighted in blue, the HNH domain is hidden for visualization purposes.

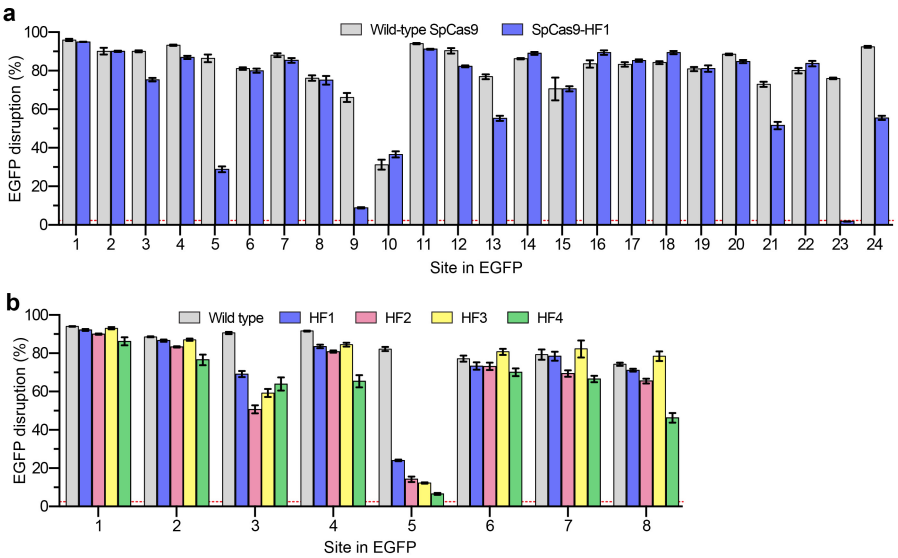


**Extended Data Figure 2 | On-target activities of high-fidelity SpCas9 variants. a**, **b**, EGFP disruption activities of wild-type SpCas9 and SpCas9-HF1 (**a**) and SpCas9-HF1-derivative variants (**b**) in human cells. SpCas9-HF1 contains N497A, R661A, Q695A, and Q926A substitutions; HF2 = HF1 + D1135E; HF3 = HF1 + L169A; HF4 = HF1 + Y450A. Error bars represent s.e.m. for $n = 3$; mean level of background EGFP loss represented by the red dashed line.

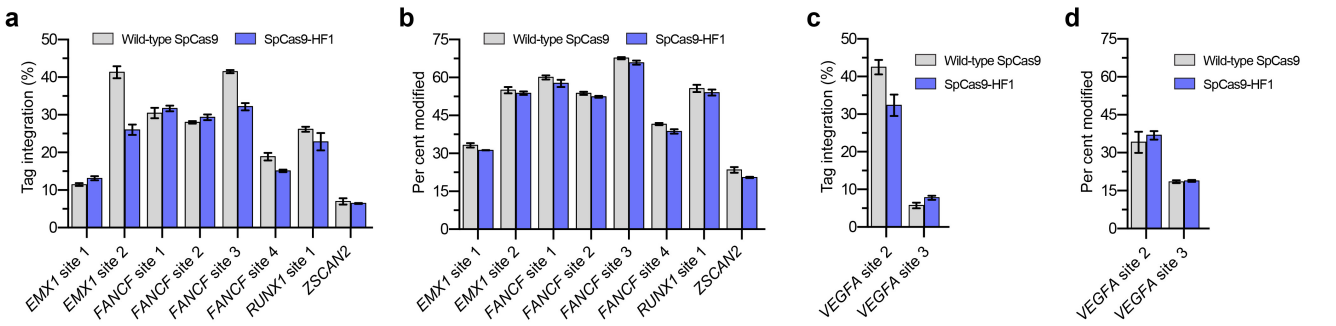


**Extended Data Figure 3 | On-target activity comparisons of wild-type and SpCas9-HF1 with various sgRNAs used for GUIDE-seq experiments. a**, **c**, Mean GUIDE-seq tag integration at the intended on-target site for GUIDE-seq experiments shown in Figs 2a and Extended Data Fig. 5 (**a** and **c**, respectively), quantified by restriction-fragment length polymorphism assay. Error bars represent s.e.m. for $n = 3$. **b**, **d**, Mean percent modification at the intended on-target site for GUIDE-seq experiments shown in Fig. 2a and Extended Data Fig. 5 (**b** and **d**, respectively), detected by T7 endonuclease I assay. Error bars represent s.e.m. for $n = 3$.

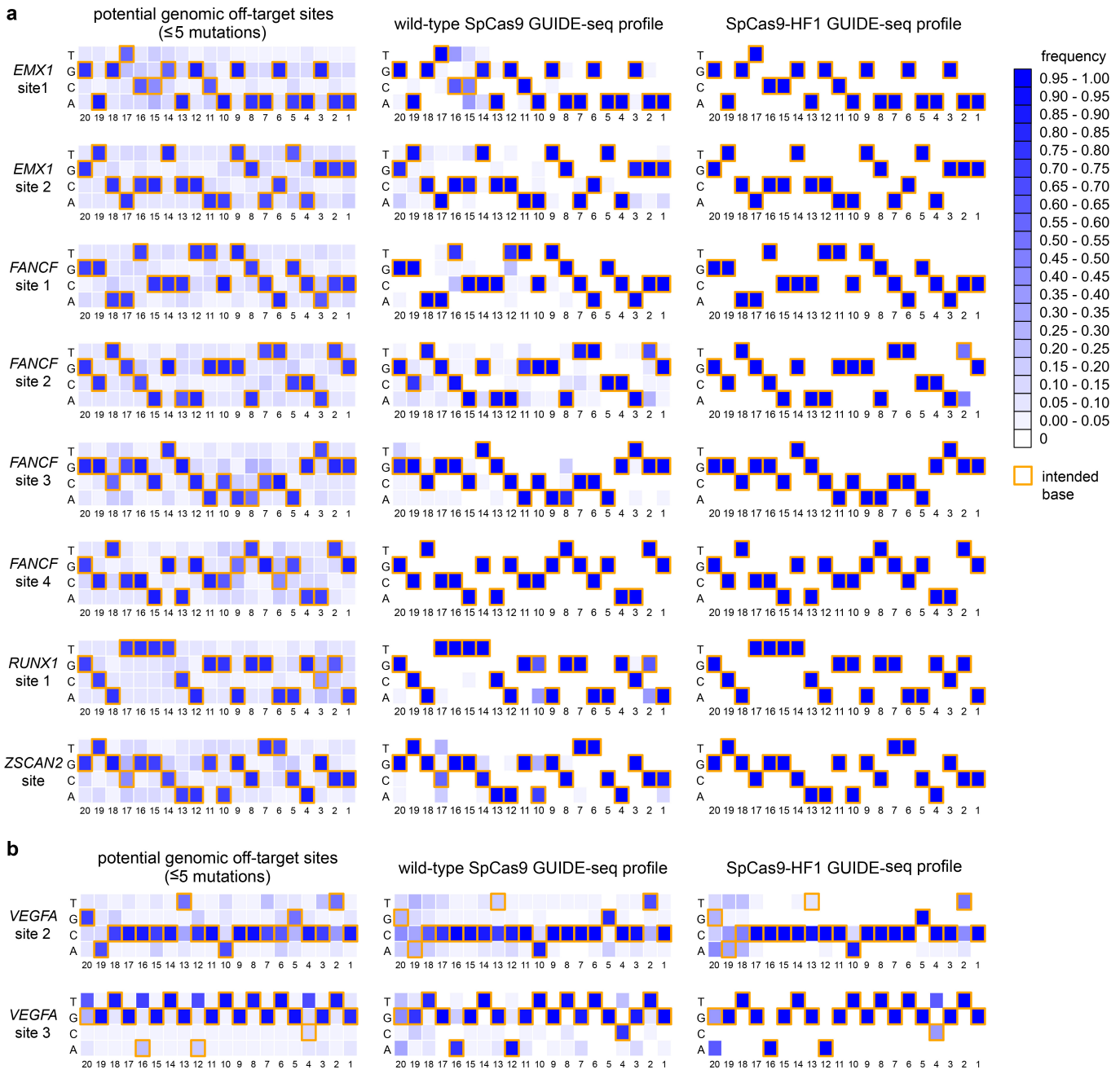


**Extended Data Figure 4 | Positional summary of off-target sites identified by GUIDE-seq. a**, **b**, Heat maps derived from GUIDE-seq data with sgRNAs targeting non-repetitive (**a**), or repetitive or homopolymeric sites (**b**) in the genome are shown. Base frequencies in the set of all potential genomic off-target sites (weighted equally) with NGG PAMs and five or fewer mutations for each sgRNA are shown on the left. Summaries of off-target sites identified by GUIDE-seq for wild-type SpCas9 and SpCas9-HF1 (both weighted by read count) are shown on the right. Yellow box outlines denote on-target bases at each position. Positions (20–1) are shown below the heat maps, with 1 being the most PAM-proximal position. Note the presence of mismatches that would be expected to create potential wobble interactions (G→A or T→C) at certain positions among the off-target sites induced by wild-type SpCas9 and that SpCas9-HF1 appears to reduce off-target activity without any obvious positional bias.

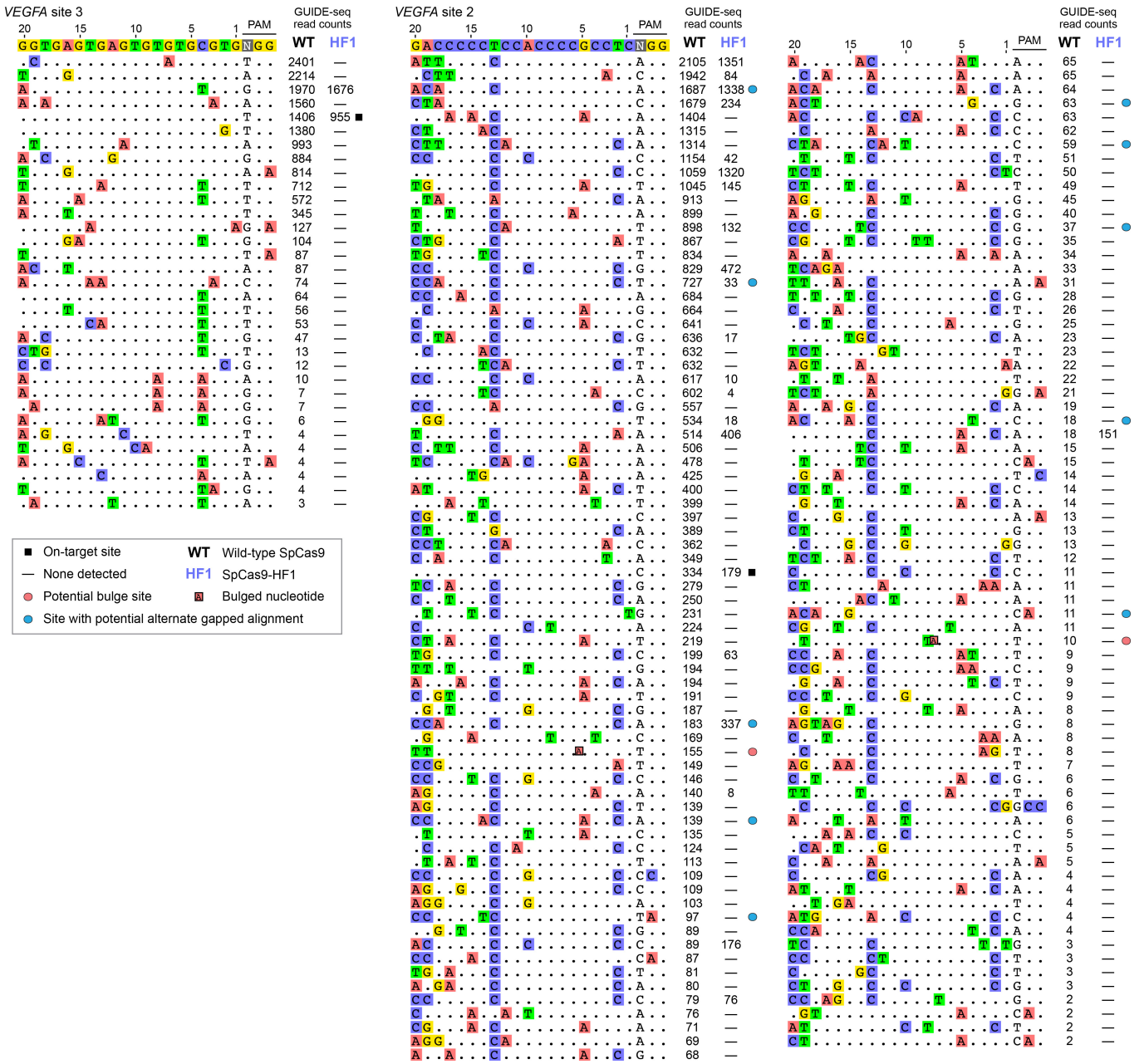


**Extended Data Figure 5 | Genome-wide cleavage specificity of wild-type SpCas9 and SpCas9-HF1 with sgRNAs targeted to non-standard, repetitive sites. a**, GUIDE-seq profiles of wild-type SpCas9 and SpCas9-HF1 using two sgRNAs known to cleave large numbers of off-target sites[4,8]. GUIDE-seq read counts represent a measure of cleavage efficiency at a given site. Mismatched positions within the spacer or PAM are highlighted in colour red circles indicate off-target sites likely to have the indicated bulge[12] at the sgRNA–DNA interface, blue circles indicate sites that may have an alternative gapped alignment relative to the one shown (see Extended Data Fig. 6). Off-target sites marked with red circles are not included in the counts of Fig. 4b, sites marked with blue circles are counted with the number of mismatches in the non-gapped alignment for Fig. 4b.

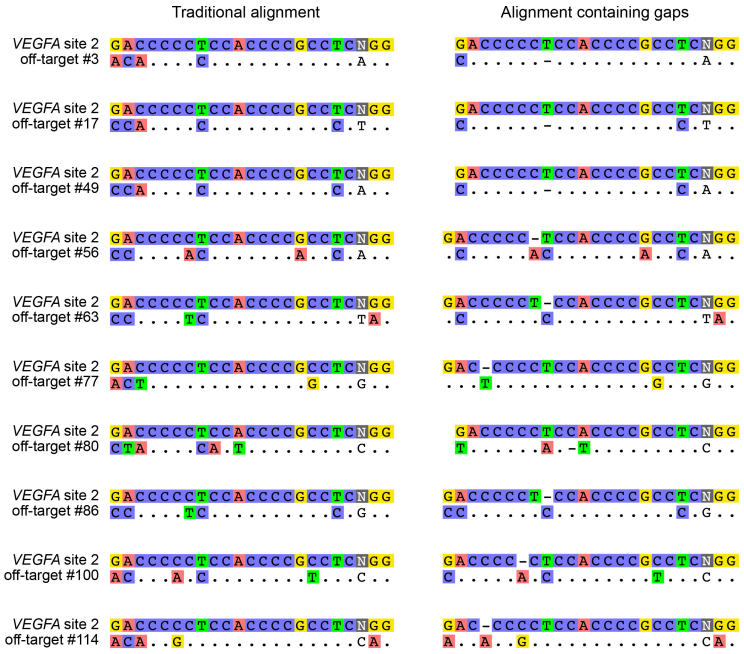


**Extended Data Figure 6 | Potential alternate alignments for *VEGFA* site 2 off-target sites.** Ten *VEGFA* site 2 off-target sites identified by GUIDE-seq (left) that may potentially be recognized as off-target sites with single nucleotide gaps[12] (right), aligned using Geneious[45] version 8.1.6 (http://www.geneious.com).

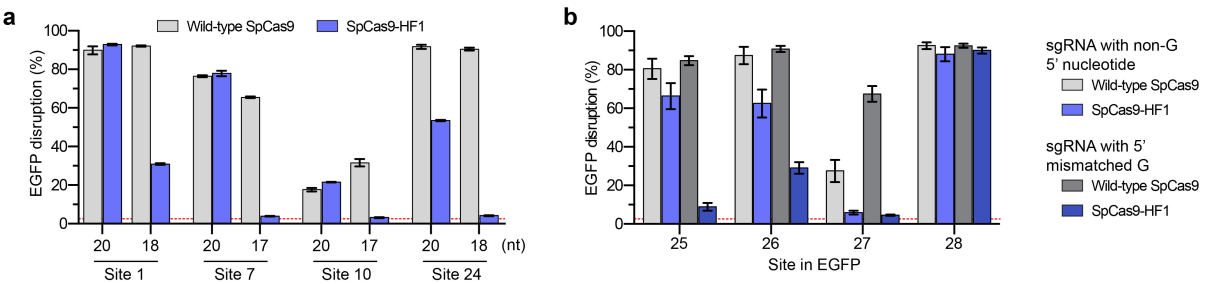


**Extended Data Figure 7 | Activities of wild-type SpCas9 and SpCas9-HF1 with truncated or 5′ mismatched sgRNAs[14].** **a**, EGFP disruption activities of wild-type SpCas9 and SpCas9-HF1 using full-length or truncated sgRNAs. **b**, EGFP disruption activities of wild-type SpCas9 and SpCas9-HF1 using sgRNAs that encode a matched 5′ non-G nucleotide or an intentionally mismatched 5′ G nucleotide. For both panels, error bars represent s.e.m. for $n = 3$, and the mean level of background EGFP loss observed in control experiments is represented by the red dashed line.

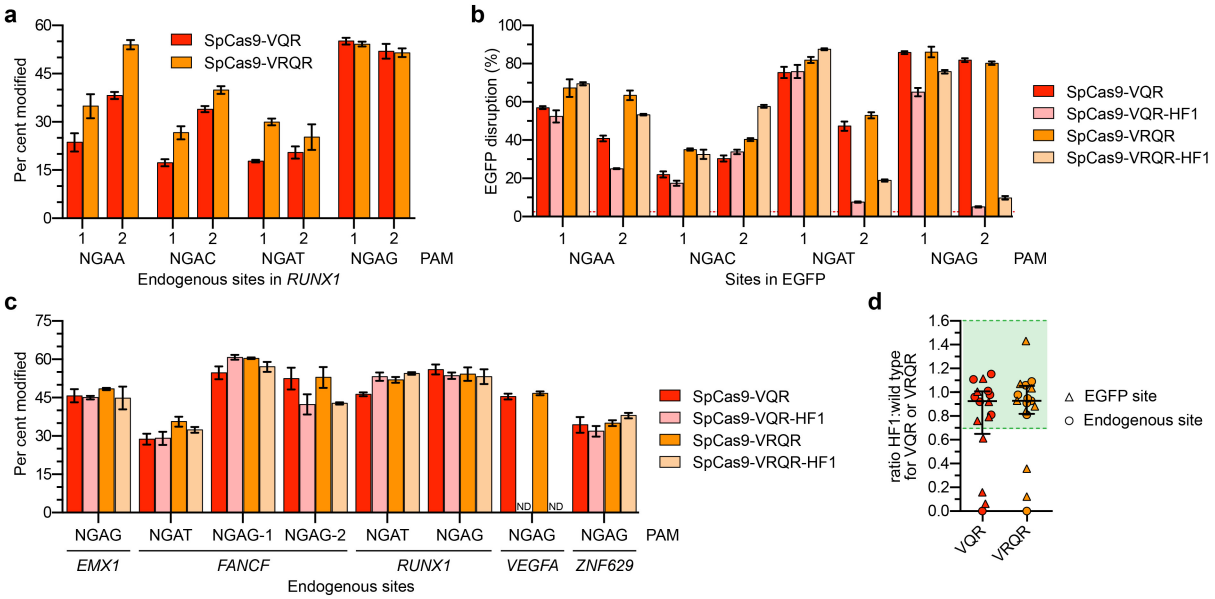


**Extended Data Figure 8 | Altering the PAM recognition specificity of SpCas9-HF1. a**, Comparison of the mean per cent modification of on-target endogenous human sites by the SpCas9-VQR variant (ref. 15) and an improved SpCas9-VRQR variant using 8 sgRNAs, quantified by T7 endonuclease I assay. Both variants are engineered to recognize an NGAN PAM. Error bars represent s.e.m. for $n = 3$. **b**, On-target EGFP disruption activities of SpCas9-VQR and SpCas9-VRQR compared to their -HF1 counterparts using eight sgRNAs. Error bars represent s.e.m. for $n = 3$; mean level of background EGFP loss in negative controls represented by the red dashed line. **c**, Comparison of the mean on-target per cent modification by SpCas9-VQR and SpCas9-VRQR compared to their -HF1 variants at eight endogenous human gene sites, quantified by T7 endonuclease I assay. Error bars represent s.e.m. for $n = 3$; ND, not detectable. **d**, Summary of the fold-change in on-target activity when using SpCas9-VQR or SpCas9-VRQR compared to their corresponding -HF1 variants (from **b** and **c**). The median and interquartile range are shown, the interval showing greater than 70% of wild-type activity is highlighted in green.

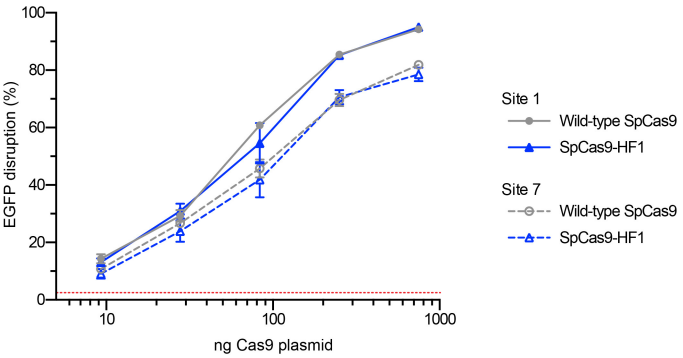


**Extended Data Figure 9 | Titrations of wild-type SpCas9 and SpCas9-HF1 expression plasmid amounts.** Human cell EGFP disruption activities from transfections with varying amounts of wild-type and SpCas9-HF1 expression plasmids. For all transfections, the amount of sgRNA-containing plasmid was fixed at 250 ng. Two sgRNAs targeting different sites were used; Error bars represent s.e.m. for $n = 3$; mean level of background EGFP loss in negative controls is represented by the red dashed line.

**Extended Data Table 1 | Summary of potential mismatched sites in the reference human genome for the ten sgRNAs examined by GUIDE-seq**

| | | mismatches to on-target site* | | | | | | |
|---|---|---|---|---|---|---|---|---|
| site | spacer with PAM | 1 | 2 | 3 | 4 | 5 | 6 | total |
| *EMX1* site 1 | GAGTCCGAGCAGAAGAAGAAGGG | 0 | 1 | 18 | 273 | 2318 | 15831 | 18441 |
| *EMX1* site 2 | GTCACCTCCAATGACTAGGGTGG | 0 | 0 | 3 | 68 | 780 | 6102 | 6953 |
| *FANCF* site 1 | GGAATCCCTTCTGCAGCACCTGG | 0 | 1 | 18 | 288 | 1475 | 9611 | 11393 |
| *FANCF* site 2 | GCTGCAGAAGGGATTCCATGAGG | 1 | 1 | 29 | 235 | 2000 | 13047 | 15313 |
| *FANCF* site 3 | GGCGGCTGCACAACCAGTGGAGG | 0 | 0 | 11 | 79 | 874 | 6651 | 7615 |
| *FANCF* site 4 | GCTCCAGAGCCGTGCGAATGGGG | 0 | 0 | 6 | 59 | 639 | 5078 | 5782 |
| *RUNX1* site 1 | GCATTTTCAGGAGGAAGCGATGG | 0 | 2 | 6 | 189 | 1644 | 11546 | 13387 |
| *ZSCAN2* | GTGCGGCAAGAGCTTCAGCCGGG | 0 | 3 | 12 | 127 | 1146 | 10687 | 11975 |
| *VEGFA* site 2 | GACCCCCTCCACCCCGCCTCCGG | 0 | 2 | 35 | 456 | 3905 | 17576 | 21974 |
| *VEGFA* site 3 | GGTGAGTGAGTGTGTGCGTGTGG | 1 | 17 | 383 | 6089 | 13536 | 35901 | 55927 |

*Determined using Cas-OFFinder (http://www.rgenome.net/cas-offinder/).